A STOCHASTIC AFTERHYPERPOLARIZATION MODEL OF REPETITIVE ACTIVITY IN VESTIBULAR AFFERENTS

Charles E. Smith and Jay M. Goldberg

Department of Statistics, Biomathematics Graduate Program,
North Carolina State University, Raleigh, North Carolina 27695

Department of Pharmacological and Physiological Sciences,
University of Chicago, Chicago, Illinois 60637

Running head: Stochastic Afterhyperpolarization Model

Correspondence to:

Dr. Charles E. Smith
Department of Statistics
Biomathematics Graduate Program
Box 8203
North Carolina State University
Raleigh, North Carolina 27695-8203

Abstract. A stochastic version of Kernell's (1968, 1972) model with cumulative afterhyperpolarization (AHP) was simulated. A characteristic of the model is that the AHP is the result of an increased potassium conductance (g_K) that is time-dependent but not voltage-dependent. Quantal synaptic inputs are assumed to be the only source of interspike-interval variability. The model reproduces many features of the steady-state discharge of peripheral vestibular afferents, provided that firing rates are higher than 40 spikes/s. Among the results accounted for are the interspike-interval statistics occurring during natural stimulation and their alteration by externally applied galvanic currents and the increase in the interspike interval following an interposed shock. Empirical studies show that some vestibular afferents have a regular spacing of action potentials, others an irregular spacing (Goldberg and Fernández, 1971b; Fernández and Goldberg, 1976). Irregularly discharging afferents have a higher sensitivity to externally applied galvanic currents than do regular afferents (Goldberg et al., 1984). To explain the relation between galvanic sensitivity and discharge regularity requires the assumption that neurons differ in both their synaptic noise (σ_V) and the slopes of their postspike voltage trajectories ($d\mu_V/dt$). The more irregular the neuron's discharge at a given firing frequency, the greater is σ_V and the smaller is $d\mu_V/dt$. Of the two factors, $d\mu_V/dt$ is estimated to be four times more influential in determining discharge regularity across the afferent population. The shortcomings of the model are considered, as are possible remedies. Our conclusions are compared to previous discussions of mechanisms responsible for differences in the discharge regularity of vestibular afferents.

1. Introduction

There is now abundant evidence that the timing of repetitive discharge of many neurons is governed by an afterhyperpolarization (AHP), based on an increased potassium conductance (Kernell, 1968, 1972; Connor, 1978; Gustafsson et al., 1978; Crill and Schwindt, 1983). Similar mechanisms most likely operate in vestibular nerve afferents (Highstein and Politoff, 1978). In this paper, we take an AHP model, one developed by Kernell (1968, 1972) to account for repetitive firing in motoneurons, and extend it to account for interspike interval variability. The stochastic version of Kernell's model is then compared with experimental data obtained from vestibular nerve afferents in the squirrel monkey (Goldberg et al., 1984). Our motivation for this theoretical exercise was related to the fact that some vestibular afferents have a regular spacing of action potentials, whereas in other afferents, the spacing is irregular (Goldberg and Fernández, 1971b; Fernández and Goldberg, 1976). Further, irregularly discharging afferents have a higher sensitivity to externally applied galvanic currents than do regular afferents (Goldberg et al., 1984). We were interested in seeing whether these differences could be explained by variations in the parameters of a simple, but physiologically realistic, model. Two parameters were of particular interest. These are the synaptic noise, σ_V, and the slope of the postspike voltage trajectory, $d\mu_V/dt$ (Stein, 1967). The regularity of discharge should be related to both factors. Galvanic sensitivity, on the other hand, should be largely determined by $d\mu_V/dt$. Since a closed form solution to the model does not exist, simulations were used to establish the combinations of $d\mu_V/dt$ and σ_V needed to reproduce the discharge regularity and galvanic sensitivity for various afferents. From these combinations, we could then estimate

the relative contributions that the two factors make in determining variations in discharge regularity across the afferent population.

2. The Model

The model, illustrated in Fig. 1, consists of three conductances in parallel with the membrane capacity (C_M) and an external current source (I_P). The conductances are a resting or leak conductance (G_L), an excitatory synaptic conductance (G_S), and a time-varying potassium conductance (G_K). G_S is proportional to the input that the sensory axon receives from hair cells. G_K is responsible for an AHP. An implicit assumption is that applied currents (I_P) act on the axon and not on the hair cell.

[INSERT FIGURE 1]

Membrane potentials (V) are measured from the resting potential and are expressed as the intracellular (V_I) minus the extracellular (V_E) potential. For numeric calculations, the equilibrium potentials are assumed to be $V_L = 0, V_S = 70$ mV and $V_K = -30$ mV. Define $g_S = G_S/G_L, g_K = G_K/G_L$, $V_P = I_P/G_L$ and $\tau_M = C_M/G_L$. The circuit equation is

$$\tau_M(dV/dt) + (1 + g_S + g_K)V(t) = g_S V_S + g_K V_K + V_P. \qquad (1)$$

The time dependence of the potassium conductance following an isolated spike is assumed to be $g_K(t) = g_{KO}\exp(-t/\tau_K)$, where t is the postspike time, $g_{KO} = g_K(t = 0)$ and τ_K is a time constant. Firing occurs whenever V(t) reaches a fixed threshold V_T. The conductance g_S is assumed to be a homogeneous shot-noise process composed of quantal events of rate λ, amplitude Δg_S, and effective duration Δt_S; the mean value ($\bar{g}_S$) and the variance $\sigma^2(g_S)$ are, based on shot-noise theory, i.e., Campbell's theorem (Rice, 1944), $\bar{g}_S = \lambda \cdot \Delta g_S \cdot \Delta t_S$ and $\sigma^2(g_S) = \Delta g_S^2 \cdot \lambda \cdot \Delta t_S = \bar{g}_S \cdot \Delta g_S$. The quantal EPSP size, measured at rest, is $A = \Delta g_S \cdot V_S$.

The salient features of the model are more easily obtained by setting the membrane time constant, $\tau_M = 0$. This is not an unreasonable assumption for our situation, since there is experimental evidence that in vestibular afferents (Schessel, 1982), as in other vertebrate axons (Tasaki, 1955), $\tau_M < 0.1$ ms, a value much shorter than the likely values of τ_K and Δt_S. With this simplification, V(t) becomes

$$V(t) = (g_S V_S + g_K(t) V_K + V_P) \; / \; (1 + g_S + g_K(t)) \; . \qquad (2)$$

Since g_S is a random process, so is V(t). The latter has a mean, $\mu_V(t)$, and a standard deviation, $\sigma_V(t)$. Equation 2 was simulated in Fortran on a Prime 550, IBM 3081 and Amdahl 470. The GGPOS subroutine of the International Mathematics and Statistical Library (1980) was used to calculate the number of quantal events in discrete time steps of 0.1 ms. V_T was always set to 10 mV and Δt_S to 0.5 ms. It was assumed that there was a cumulative summation of AHPs: a definite proportion (p) of the g_K left over from preceding activity was added to the g_K triggered by each spike. By analogy with other repetitively discharging neurons (Kernell, 1972; Gustafsson and Zangger, 1978), we made p = 1 in all cases.

Four parameters determine the properties of the model neuron. Three of these -- g_{KO}, τ_K and p -- specify the AHP. The fourth is the quantal EPSP size (A). All four parameters remained fixed for a given neuron. The discharge rate of the neuron was modulated by natural and electrical stimulation, which were mimicked by varying g_S and V_P, respectively. We first investigated whether variations in discharge regularity and in galvanic sensitivity could be explained if units only differed in their g_{KO} values. Discharge regularity was measured by a normalized coefficient of variation (cv^*), appropriate to a mean interval of 15 ms. Units with $cv^* < 0.1$ are called *regular*; those with $cv^* > 0.2$,

irregular; and those in between *intermediate* as in Goldberg et al. (1984). Sensitivity to external galvanic currents was expressed as a factor (β_p) with dimensions of spikes·s^{-1}/mV. A discrepancy was encountered. The predicted relation between β_p and cv* was too steep or, put another way, the dependency of cv* on g_{KO} was too weak. To overcome the discrepancy, we had to assume that units differed in both their AHPs and in their quantal sizes: the more irregular the neuron, the lower was its g_{KO} and the higher its A. Finally, g_{KO} and τ_K were adjusted to provide a good visual match to the empirical interval statistics obtained during natural stimulation. Table 1 summarizes the model parameters for five units with cv*s ranging from 0.026 to 0.51 in roughly octave steps.

[INSERT TABLE 1]

3. Simulation Results

3.1 Interval Statistics During Natural Stimulation

The simulated relations between the coefficient of variation (cv) and the mean interval ($\bar{t}$) are shown in Fig. 2 as points. The solid curves are the corresponding empirical relations generated from a large population of vestibular afferents innervating the otolith organs (Goldberg et al., 1984). The predicted cv becomes too large as $\bar{t}$ increases beyond 25 ms. The discrepancy is large for regular neurons (units 1-3), becomes smaller for unit 4, and disappears for the most irregular unit (unit 5). In other respects, the agreement between experiment and theory is satisfactory. The model accounts for the fact that the curves for regular units are U-shaped, whereas those for irregular units increase monotonically with mean interval.

[INSERT FIGURE 2]

Model units 1-5 differ in both their AHPs and their quantal size. To identify the separate influences of these factors, two additional neurons pairs were studied (see Table 1). In one pair (units 3A, B), only the quantal size (A) was varied; in the other pair (units 3C, D), only AHP parameters (g_{K0} and τ_K) were changed. The separate variations were identical to those used in combination in units 1 and 5. For the parameters used in the simulations, variations in AHP and in quantal size both affect discharge regularity, but not to the same extent. The ratio of cv*s for units 3C-D is four times the ratio for units 3A-B.

This last result can be stated in terms of the two factors considered in the INTRODUCTION. The regularity of discharge should be directly related to σ_V, the standard deviation of the voltage process, and inversely related to $d\mu_V/dt$, the slope of the postspike voltage trajectory (Stein, 1967). The two variables, evaluated at a mean interval of 10 ms, are included in Table 1. As is exemplified by the table, σ_V is almost entirely determined by quantal size, whereas $d\mu_V/dt$ is similarly related to g_{K0} and τ_K. Hence, $d\mu_V/dt$ is four times more influential than is σ_V in causing variations in discharge regularity across the model population.

3.2 Interval Statistics During Galvanic Currents

The model accounts for the observed effects of external currents on interval statistics (Goldberg, Smith and Fernández, unpublished observations). The dashed lines in Fig. 2 show the cv vs $\bar{t}$ relation when the background mean interval, $\bar{t}_0$ = 10 ms, was modified by varying V_p, while keeping $\bar{g}_S$ constant. Excitatory galvanic currents decrease cv below the values obtained during natural stimulation; inhibitory currents has the opposite influence. The changes in cv are well fit by the same power law that can be used in describing experimental data. Suppose that the background

mean interval, $\bar{t}_0$, is changed to $\bar{t}_1$ by either natural or electrical means. The relations between cv and $\bar{t}$ can be represented locally by the power law

$$cv_P(\bar{t}_1)/cv_N(\bar{t}_1) = (\bar{t}_1/\bar{t}_0)^q, \quad (3)$$

where the subscripts refer to galvanic polarization (P) and natural stimulation (N) and q is an empirically determined exponent. From Table 1, the simulation results provide q values of 0.4-0.7 for regular neurons (units 1-3) and closer to 0.1-0.3 for irregular neurons (units 4-5). Similar results were obtained when the simulated mean interval was set to 7 or to 14 ms. The corresponding empirical values have a mean $\pm$ S.E.M. of 0.42 $\pm$ 0.10 and 0.12 $\pm$ 0.10 for regular and irregular units, respectively (Goldberg, Smith and Fernández, unpublished results). The small change in cv can be explained as follows. An excitatory natural stimulus will increase the quantal release rate and, hence, the synaptic noise, σ_V; an inhibitory natural stimulus should have the opposite effect. A galvanic current, provided that it acts directly on the afferent terminal, will not change the quantal rate or σ_V. Were this the only factor involved, an excitatory natural stimulus should lead to a more irregular discharge and an inhibitory natural stimulus should result in a more regular discharge than would the corresponding galvanic currents.

3.3. Interspike Voltage Trajectories and Discharge Regularity

[INSERT FIGURE 3]

Firing may be termed *deterministic* or *nondeterministic* according to whether the mean postspike voltage trajectory (μ_V) does or does not cross the threshold voltage (V_T). The two types of discharge are illustrated in Fig. 3, which includes voltage trajectories for model units 2 (Fig. 3A) and 5 (Fig. 3B). When the firing is deterministic (Fig. 3A), the mean interval corresponds closely to the point in time where μ_V crosses V_T

and discharge would occur even in the absence of synaptic noise. Here, the discharge can be regular. For nondeterministic firing (Fig. 3B), μ_V remains below V_T and spikes occur only because there is synaptic noise, which varies from one interspike interval to the next. Here, the discharge is irregular. Unit 2 is regular; unit 5, irregular. The differences in their simulated trajectories are qualitatively similar to those observed in a lizard crista (Schessel, 1982) in that the trajectory for the regular unit has a prominent hyperpolarizing-depolarizing sequence, whereas that for the irregular unit is relatively flat. As firing rate is lowered, however, the distinction between regular and irregular units is obscured. Unit 2 can be cited as an example. For rates between 0-40 spikes/s, the discharge becomes nondeterministic, the interspike trajectory becomes relatively flat during much of the interspike interval, and the discharge becomes irregular. Above 40 spikes/s, the discharge becomes deterministic. In contrast, the discharge for unit 5 remains nondeterministic for rates as high as 225 spikes/s. The main difference, in fact, between regular and irregular neurons is that, for the latter, nondeterministic firing, rather than being confined to low rates, extends throughout much of the physiological range of firing.

3.4 Responses to Synaptic and Applied Currents

[INSERT FIGURE 4]

The relations between synaptic input ($\bar{g}_S^*$) and discharge rate are seen in Fig. 4A for model units 1-5. The abscissa is normalized so that $\bar{g}_S^* = 1$ would just bring the mean voltage trajectory (μ_V) to the firing threshold (V_T) asymptotically. The input-output curves are linear at high rates, but are concave downward at low rates. The nonlinearity becomes more conspicuous, the more regular the neuron. The model is thus at variance

with experimental input-output curves, which are linear or concave upward below 100 spikes/s (Goldberg and Fernández, 1971a; Fernández and Goldberg, 1976). The discrepancy might be explained were it assumed that the curve relating mechanical input to hair cell output is concave upward in the lower part of the hair cell's operating range. Although there is experimental evidence for such a nonlinearity (Hudspeth and Corey, 1977), it cannot provide the entire explanation. Figure 4B shows the model's input-output curves for applied currents. Here, too, the model curves are concave downward, whereas the experimental curves are concave upward (Goldberg et al., 1984). Presumably, the currents work directly on the axon's trigger site and thus bypass hair cell nonlinearities. Another possible explanation will be considered in the DISCUSSION.

The model's sensitivities to synaptic and external currents increase, the more irregular is the neuron's discharge (Fig. 4A,B). Sensitivities were estimated by calculating regression slopes from the linear parts of the corresponding input-output curves. For synaptic sensitivity (β_S), discharge rates between 50-150 spikes/s were used. Responses of $\pm$ 20 spikes/s were employed in estimating sensitivity to applied currents (β_p). Both sensitivity measures are plotted in Fig. 5A against discharge regularity (cv*). β_p is shown with solid symbols; β_S, with open symbols. Consider β_p first. A power-law regression, $\beta_p = a\ (cv^*)^b$, done on units 1-5 (●-●) gave an exponent b = 1.05, indistinguishable from that obtained experimentally. The points in Fig. 5A were for a background mean interval, $\bar{t}_0$ = 10 ms. Quite similar relations were obtained for $\bar{t}_0$'s of 7 and 14 ms. When only AHP parameters are varied (units 3C, D; Fig 5A, ■-■), a steeper relation (b =1.45) was obtained. Variation in synaptic noise (units 3A, B; Fig. 5A, ▲-▲) had only a small effect on β_p.

[INSERT FIGURE 5]

The relation between β_S and cv* is similar to that between β_P and cv* (Figure 5A). This is to be expected, since the relation, $\beta_P = \beta_S/(V_S - V_T)$, can be deduced theoretically.

3.5 Lengthening Effect of an Interposed Spike

When a shock-evoked spike is interposed in a regular discharge train, the next interspike interval is longer than it would otherwise be (Goldberg et al., 1984). Denote the mean interval between the interposed and the following spike as $\bar{t}_f$, where f is the time of the interposed spike, expressed as a fraction of the background mean interval. The lengthening effect was measured by plotting $L_f = (\bar{t}_f - \bar{t}_{7/8})/\bar{t}_0$ vs f. Experimentally, the lengthening can be 20-30% for f = 1/8.

The lengthening effect can be explained by a summation of the g_k's from closely spaced spikes. In the simulations, we assumed that the summation was linear (p = 1). The solid curve in Fig. 5B is the simulated relation between L_f and f for $\bar{t}_0$ = 10 ms; the solid points are the corresponding experimental data (Goldberg et al., 1984). There is a reasonable match between theory and experiment. The one discrepancy is that the model does not reproduce the sudden decline in L_f, sometimes to near-zero values, that occurs for interposed intervals less than 0.9 ms. The decline is responsible for the fact that the experimental point in Fig. 5B for f = 1/8 is somewhat lower than expected.

The dashed lines in Fig. 5B are the simulated relations for $\bar{t}_0$ = 7 ms (above) and $\bar{t}_0$ = 14 ms (below). The decrease in L_f with increasing $\bar{t}_0$ is similar to that actually observed (Goldberg, Smith and Fernández, unpublished observations).

3.6 Postspike Recovery Functions

[INSERT FIGURE 6]

Recovery functions were measured in our experiments by determining the thresholds to cathodal shocks, 50 μs in durations, presented at various postspike times (Goldberg et al., 1984). To compare these results with those from the model, we computed shock thresholds for postspike time, t, by the formula $V_P = \{V_T - \mu_V(t)\} \cdot \{1 + \bar{g}_S + g_K(t)\}$, gotten by rearrangement of equation 2. Recovery functions for model units 1, 3 and 5 are presented in Fig. 6A. The model resembles experiment in three ways. First, regular units have higher thresholds than do irregular units. The difference in $T_{1/2}$, the threshold at f = 1/2, calculated for different model units is slightly smaller than expected. We found that our experimental data was fit by a power law, $T_{1/2} = a \cdot (cv^*)^b$, with b = -0.79. Model units differ in their cv*'s by a factor of 19.2, so their $T_{1/2}$'s should differ by $(19.2)^{0.79}$ or about 10x. The calculated difference in $T_{1/2}$ is 7.6 at 10 ms (Fig. 6A). Second, the curves obtained from an individual unit are similar in their shapes despite variations in mean interval. Third, the recovery functions measured near the mean interval are relatively flat for irregular units and relatively steep for regular units.

There is, at the same time, a discrepancy between the shapes of the recovery functions obtained from the model and from experiment. In the model, the recovery functions for all units are concave upward (Fig. 6A). In actual fact, the curves for regular units are concave downward, those for intermediate units close to linear, and only those for irregular units concave upward (Goldberg et al., 1984). The currents are thought to modify discharge by acting on the physiological trigger site. They do so, in part, because the trigger site is under the influence of depolarizing

synaptic currents and, hence, is more excitable than the proximal axon. Such a mechanism will operate during later parts of the interspike interval when synaptic currents have brought the trigger site close to its firing level. Earlier in recovery, the trigger site can be hyperpolarized by the AHP beyond its resting potential and, hence, would be less excitable than more proximal zones. A shock-evoked response occurring early in recovery could thus be initiated proximally. Since the recovery function of the proximal axon is quite fast (Goldberg et al., 1984), this could explain why the recovery functions of regular units are relatively flat during early parts of the interspike interval, when the spike is initiated proximally, and steep during later parts of the interval, when the currents act distally.

To explore this idea, we studied a distributed model obtained by combining circuit equations that describe the response of fibers to externally applied currents (BeMent and Ranck, 1969; Bean, 1974) with our basic model. We assumed that the trigger site was located at the proximal end of an unmyelinated terminal, which continued as a myelinated fiber. The firing thresholds, V_T, were set to 10 mV for the trigger site and 25 mV for each node of the myelinated fiber. The conductances, $\bar{g}_S$ and g_k, were uniformly distributed throughout the terminal. The voltages they generate should still be approximated by equation 2 at the trigger site and should decrease exponentially with distance from the trigger site as one proceeds proximally along the myelinated fiber (Rall, 1962). Figure 6B shows recovery functions for the distributed model. The shapes of the recovery functions are more in accord with experiment. The ratio between the $T_{1/2}$'s for units 1 and 5, however, is reduced to 2.8x,

considerably different from experiment. Other shortcomings of the distributed model will be considered in the next section.

4. Discussion

4.1. Evaluation of the model.

Our extension of Kernell's model is based on four major assumptions. First, there is a single trigger site in each axon and a spike occurs whenever the transmembrane depolarization at the site reaches a critical firing level, V_T. Second, depolarization is contributed by quantal EPSPs, whose discrete nature and random timing lead to synaptic noise. Consequently, postspike voltage trajectories will fluctuate from one interspike interval to the next. These fluctuations are the only source of interspike-interval variability. Third, external currents influence discharge by acting at the trigger site, rather than on hair cells or on the axon far distant from the epithelium. Fourth, each spike results in an increased potassium conductance (g_K) and a consequent afterhyperpolarization (AHP). The conductance is time dependent, but not voltage dependent. It declines exponentially after each spike with a time constant, τ_K. There is a summation of the g_K's left over from previous activity with that arising from individual action potentials. Similar assumptions have been made in models used to simulate the discharge of motoneurons (Kernell, 1968, 1972; Baldisserra and Gustafsson, 1974; MacGregor and Oliver, 1974; Baldissera et al., 1976) and of dorsal spinocerebellar tract neurons (Gustafsson et al., 1978). The one novel feature of the present model is that, by taking into account the shot-noise nature of synaptic input, we have been able to account for interspike interval variability. The evidence that the assumptions are appropriate for vestibular afferents was reviewed in another paper (Goldberg et al., 1984) and need not be

repeated here. Rather, we shall consider the adequacy of the model in describing our experimental results.

Despite the relative simplicity of the model, it simulates many features of the steady-state discharge of vestibular afferents, provided that the firing rate is high. Among the results accounted for are: the interspike-interval statistics obtaining during natural stimulation and their alteration by galvanic currents, the relation between discharge regularity and galvanic sensitivity, the lengthening effect of an interposed spike, and the difference in interspike-interval voltage trajectories and in short-shock thresholds of regular and irregular units.

One result not accounted for by the model is the sudden decline in the lengthening effect when the interposed spike falls less than 1 ms after the last naturally occurring action potential. This discrepancy is easily explained. In many neurons (Barrett and Barrett, 1976; Crill and Schwindt, 1983), each spike has both a sodium (Na) and a calcium (Ca) component and the AHP is the result of an outward $I_{K(Ca)}$, a Ca-activated potassium (K) current. One feature of such a process is that the inward Ca produced by each spike summates with the residual Ca left over from preceding activity. Presumably, the potassium conductance, g_K, is proportional to intracellular Ca, which would then disappear with an exponential time course. Most of the residual Ca is contributed by the immediately preceding spike. We can now consider the case of an interposed spike. The shorter the interval terminated by an interposed spike, the greater is the residual Ca, the larger is the g_K and the AHP following the interposed spike, and the more pronounced is the lengthening effect (Fig. 5B). But the interposed spike, were it to fall within the refractory period of the preceeding spike, should be smaller than normal, as should be the inward Ca current,

the outward $I_{K(Ca)}$, and the AHP. Conceivably, if the interposed spike were sufficiently small, it could fail to trigger $I_{K(Ca)}$ and the lengthening effect would disappear or be replaced by a shortening of the next interspike interval.

The model does less well when the rate falls below approximately 40 spikes/s. Specifically, the simulated cv's are too large for mean intervals longer than 25 ms. Moreover, the input-output curves obtained from the model, including those for natural and galvanic stimulation, show a nonlinearity at low rates that is not encountered experimentally. Both discrepancies are more conspicuous for regular, than for irregular, units and may have a common origin. We have assumed that g_K is a purely time-dependent process, such that the slope ($d\mu_V/dt$) of the AHP will decrease with time and will approach zero for times much longer than τ_K. The sensitivity, given by the slope of the input-output curve, and the standard deviation of intervals are both inversely related to $d\mu_V/dt$ (Stein, 1967). Increasing the slope of the voltage process at low rates will serve to linearize the input-output curve and to regularize the discharge. An AHP based on an I_A process could accomplish this. I_A is a potassium current, described in both invertebrate (Connor and Stevens, 1971; Connor, 1978) and vertebrate neurons (Gustafsson et al., 1982; Crill and Schwindt, 1983), which becomes activated when the membrane is repolarized after an action potential, reaches a maximum, and then becomes inactivated as depolarizing currents bring the membrane potential towards the firing threshold. One consequence of this voltage-dependent behavior is that constant currents can give rise to a slow AHP and slow repetitive activity, even though the underlying conductance change has fast kinetics when measured under voltage-clamp conditions. While an I_A

process might explain the low-firing rate behavior of vestibular afferents, it is unclear that it could account for the lengthening effect. For this reason, it might be suggested that the AHPs, at least those of regular vestibular afferents, are the result of both I_A and $I_{K(Ca)}$currents. The suggestion has precedence, since some mammalian cells possess both kinds of currents (Gustafsson et al., 1982; Crill and Schwindt, 1983). At the same time, our experimental results are consistent with an $I_{K(Ca)}$ being entirely responsible for the smaller, faster AHPs of irregular units. For the latter units, the input-output curves are linearized by the presence of synaptic noise with relatively large values of σ_V (Stein, 1967).

One discrepancy of the present model involves the shape of the postspike recovery functions measured even at high rates. Specifically, the short-shock thresholds for regular units remain relatively constant early in the interspike interval and decline rapidly only for postspike times greater than half the mean interval. The model does not reproduce the early, plateau portion of the recovery function. The discrepancy will not alter the firing behavior of regular neurons, since spikes do not occur during the early plateau. One explanation for the discrepancy involves the assumed time course for g_K. Kernell's (1968, 1972) model has a g_K with a simple exponential decline. Experimentally observed AHPs and the associated g_K's usually show an early plateau. This is so whether the AHP is the result of an I_A (Connor and Stevens, 1971; Connor, 1978) or an $I_{K(Ca)}$ current (Baldiserra et al., 1974, 1976). An early plateau in g_K would cause an early plateau in short-shock thresholds.

Another, by no means mutually exclusive, explanation for the early plateau is that the trigger site for external shocks could move from the proximal axon to the unmyelinated terminal during the course of the

interspike interval. A distributed version of our model had precisely this behavior. While the shapes of the recovery functions were qualitatively reproduced, the distributed model had its own difficulties. The differences in short-shock threshold, $T_{1/2}$, between regular and irregular units were much smaller than observed empirically. Another discrepancy, not illustrated in the RESULTS, concerned the effects of external galvanic currents on interval statistics, which were now too small. The two difficulties may result from the same feature of the distributed model. The influence of external currents on the membrane potential (V) depends on the sum of the membrane conductances, $\Sigma g = 1 + g_K + g_S$. In our original model, V is inversely proportional to (Σg), whereas in the distributed model it is inversely proportional to $(\Sigma g)^k$, $k < 1$. While the value of k depends on the other assumed parameters, for most reasonable choices, k was close to 0.5. The circuit equations used in the distributed model were adaptations of those used to explain the responses to electric shocks of purely myelinated fibers (BeMent and Ranck, 1969; Bean, 1974). If the equations are correct, the original model should be altered to account for the reduced value of k. On the other hand, in deriving the circuit equations, simplifying assumptions are made about the extracellular medium, including that it is infinite, homogeneous and isotropic. Possibly, the assumptions are inappropriate to our experimental situation.

4.2 Basis of discharge regularity

The present research began with a consideration of the cellular mechanisms that might determine discharge regularity in vestibular afferents. Two factors were identified. One is the slope of the postspike voltage trajectory, $d\mu_V/dt$; the other is the synaptic noise, σ_V. If there were a significant variation in $d\mu_V/dt$ across afferents, then two predictions

should hold. First, discharge regularity and galvanic sensitivity should be correlated: the more irregular an afferent's discharge, the greater should be its galvanic sensitivity. Second, the recovery functions of irregular afferents should be fast, whereas those of regular afferents should be slow. Experiments confirmed both predictions (Goldberg et al., 1984). Clearly, $d\mu_V/dt$ is important in determining whether an afferent has a regular or an irregular discharge. But the experimental observations do not exclude the possible importance of σ_V or provide an estimate of the relative roles of the two factors. It was for this reason that we turned to theoretical studies. The model that was developed indicates that both factors contribute. Of the two, $d\mu_V/dt$ is four times more influential than is σ_V in determining variations in discharge regularity. But we have seen that the model does not fit all of the data. Even if it did, this would not guarantee that its assumptions were correct.

In the last section, two possible revisions of the model were suggested. Neither of them would alter our basic conclusions. The first had to do with the currents responsible for the AHP. The behavior of the model depends on the magnitude of g_K, not the specific mechanism responsible for it. Substitution of an I_A for an $I_{K(Ca)}$ current might alter the values of g_K at long interspike times, corresponding to low rates of discharge. But at rates above 40 spike/s, where most of our experimental data were collected, the original model fits the data. Hence, regardless of which current is chosen, the assumed values of g_K would have to be similar, as would the relative contributions of $d\mu_V/dt$ and σ_V. The second revision, a distributed model, would actually increase the relative contribution of $d\mu_V/dt$. To see this, consider the case where all neurons have synaptic inputs with the same quantal size. The influence of an applied current

on membrane potential (ΔV) is less dependent on membrane conductance (Σg) in the distributed model ($\Delta V \propto (1/\Sigma g)^k$, $k < 1$) than in the original model ($\Delta V \propto 1/\Sigma g$). The result is that the relation between galvanic sensitivity (β_p) and discharge regularity (cv*), while still supralinear in the distributed model, is less so than in the original model. The variations in quantal size required to make the relation between β_p and cv* linear, rather than the 14x needed in the original model, is closer to 4x. The slope, $d\mu_V/dt$ would then be some eight times more important than would σ_V.

While these comments are reassuring there is no substitute for direct observation. What is required are intracellular recordings from sensory axons close to the sensory epithelium so that their intrinsic physiology, the properties of their synaptic input, and their discharge regularity can be correlated. Intracellular recordings have been made from afferents in the goldfish sacculus (Ishii et al., 1971, Furukawa et al., 1978), in the frog posterior crista (Rossi et al., 1977, 1980), and in the horizontal crista of a lizard (Schessel, 1982). In only the last study were the mechanisms of discharge regularity considered and, here, as in the other studies, almost all the recordings were obtained from thick, irregularly discharging fibers. Hopefully, the present model can serve to guide experiments when, and if, adequate recordings can be made from both regular and irregular afferents.

Most discussions of the mechanisms responsible for differences in the discharge regularity of vestibular afferents have been concerned with presumed differences in the morphology of regular and irregular afferents, including the types of hair cells innervated (Goldberg and Fernández, 1971b), the diameters of the parent axons (Walsh et al., 1972; Yagi et al., 1977), the zones of the sensory epithelium innervated (Yagi et al., 1977)

or the extent of branching within the epithelium (Walsh et al., 1972; Goldberg and Fernández, 1977; Yagi et al., 1977). A recent morphophysiological study has confirmed that regular and irregular afferents differ in the ways suggested (Goldberg et al., 1985). The conclusion of the present paper is that the major determinant of discharge regularity is an AHP that governs the postspike voltage trajectory of the sensory axons. Differences in the AHP of the fibers should reflect ionic channels residing in the unmyelinated terminals of the various fibers. If this reasoning is correct, then the various morphological features that have been considered, while they may be correlated with discharge regularity, are unlikely to be casually related to it. One possible exception involves intraepithelial branching patterns. The branches, by virtue of their cable properties, could attenuate the quantal synaptic currents that pass from distal synapses to the trigger site, thought to be located near the axon's entry into the epithelium. There can be little attenuation in some irregular afferents, those that end abruptly as individual calyces (Goldberg et al., 1985). If our models are correct, the reduction in quantal size in even regular units should be limited, amounting to some 14x in our original model and some 4x in our distributed model. Morphological studies show that the branching patterns are circumscribed, with the most distal synapse being only some 50-100 μm from the parent axon (Fernández, Baird and Goldberg, unpublished observations). At the same time, the terminal branches can be quite thin, well under 1 μm in diameter. Whether the short, but thin branches result in electrotonic decrements of the magnitude called for by our models remains to be determined. Perhaps a more intriguing question that remains unanswered concerns the roles played in sensory processing by the various kind of hair cells and the associated synapses.

Acknowledgements: This research was supported by Grants NS 01330 from the National Institutes of Health, NAG 2-148 from the National Aeronautics and Space Administration, N00014-85-K0105 from the Office of Naval Research, and Biomedical Research Support Grant RR07071. J. M. Goldberg is a Javits Neuroscience Investigator of the National Institutes of Neurological and Communicative Diseases and Stroke.

References

Baldissera, F., Gustafsson, B.: Firing behaviour of a neurone model based on the afterhyperpolarization conductance time course and algebraic summation. Adaptation and steady state firing. Acta Physiol. Scand. **92**, 27-47 (1974)

Baldissera, F., Gustafsson, B., Parmiggiani, F.: A model for refractoriness accumulation and secondary range firing in spinal motoneurons. Biol. Cybern. **24**, 61-65 (1976)

Barrett, E. F., Barrett, J. N.: Separation of two voltage-sensitive potassium currents and demonstration of a tetrodotoxin-resistant calcium current in frog motoneurones. J. Physiol. (Lond.) **255**, 737-774 (1976)

Bean, C. P.: A theory of microstimulation of myelinated axons. Appendix to Abzug, C., Maeda, M., Peterson, B. W., Wilson, V. J.: Cervical branching of lumbar vestibulospinal axons. J. Physiol. (Lond.) **243**, 499-522 (1974)

BeMent, S. L., Ranck, J. B., Jr.: A model for electrical stimulation of central myelinated fibers with monopolar electrodes. Exp. Neurol. **24**, 171-186 (1969)

Connor, J. A.: Slow repetitive activity from fast conductance changes in neurons. Fed. Proc. **37**, 2139-2145 (1978)

Connor, J. A. Stevens, C. F.: Prediction of repetitive firing behaviour from voltage clamp data on an isolated neurone soma. J. Physiol. (Lond.) **213**, 31-53 (1971)

Crill, W. E., Schwindt, P. C.: Active currents in mammalian central neurons. Trends Neurosci. **6**, 236-240 (1983)

Fernández, C., Goldberg, J. M.: Physiology of peripheral neurons innervating otolith neurons of the squirrel monkey: I. Response to static tilts and to long-duration centrifugal force. J. Neurophysiol. **39**, 970-984 (1976)

Furukawa, T., Hayashida, Y., Matsuura, S.: Quantal analysis of the size of excitatory post-synaptic potentials of synapses between hair cells and afferent nerve fibres in goldfish. J. Physiol. (Lond.) **276** 211-226 (1978)

Goldberg, J. M., Fernández, C.: Physiology of peripheral neurons innervating semicircular canals of the squirrel monkey. I. Resting discharge and response to constant angular accelerations. J. Neurophysiol. **34**, 635-660 (1971a)

Goldberg, J. M., Fernández, C.: Physiology of peripheral neurons innervating semicircular canals of the squirrel monkey. III. Variations among units in their discharge properties. J. Neurophysiol. **34**, 676-684 (1971b)

Goldberg, J. M., Fernández, C.: Conduction times and background discharge of vestibular afferents. Brain Res. **122**, 545-550 (1977)

Goldberg, J. M., Baird, R. A., Fernández, C.: Morphophysiological studies of the mammalian vestibular labyrinth. In: Contemporary Sensory Neurobiology. Correia, M. J., Perachio, A. A. eds. New York: Alan R. Liss, 231-245 (1985)

Goldberg, J. M., Smith, C. E., Fernández, C.: Relation between discharge regularity and responses to externally applied galvanic currents in vestibular nerve afferents of the squirrel monkey. J. Neurophysiol. **51**, 1236-1256 (1984)

Gustafsson, B., Galvan, M., Grafe, P., Wigstrom, H.: A transient outward current in a mammalian central neurone blocked by 4-aminopyridine. Nature (Lond.) **299**, 252-254 (1982)

Gustafsson, B., Lindström, S., Zangger, P.: Firing behaviour of dorsal spinocerebellar tract neurones. J. Physiol. (Lond.) **275**, 321-343 (1978).

Gustafsson, B., Zangger, P.: Effect of repetitive activation on the after-hyperpolarization in dorsal spinocerebellar tract neurones. J. Physiol. (Lond.) **275**, 303-319 (1978)

Highstein, S. M., Politoff, A. L.: Relation of interspike baseline activity to spontaneous discharges of primary afferents from the labyrinth of the toadfish, *Opsanus tau*. Brain Res. **150**, 182-187 (1978)

Hudspeth, A. J., Corey, D. P.: Sensitivity, polarity, and conductance change in the response of vertebrate hair cells to controlled mechanical stimuli. Proc. Natl. Acad. Sci. USA **74**, 2407-2411 (1977).

International Mathematics and Statistical Library Reference Manual, 8th edition, vol. 2, Houston, Texas: International Mathematics and Statistical Library, Inc. (1980)

Ishii, Y., Matsuura, S., Furukawa, T.: Quantal nature of transmission at the synapse between hair cells and eighth nerve fibers. Jap. J. Physiol. **21**, 79-89 (1971)

Kernell, D.: The repetitive impulse discharge of a simple neurone model compared to that of spinal motoneurones. Brain Res. **11**, 685-687 (1968).

Kernell, D.: The early phase of adaptation in repetitive impulse discharges of cat spinal motoneurones. Brain Res. **41**, 184-186 (1972)

MacGregor, R. J., Oliver, R. M.: A model for repetitive firing in neurons. Kybernetik **16**, 53-64 (1974)

Rall, W.: Theory of physiological properties of dendrites. Ann. N. Y. Acad. Sci. **96**, 1071-1092 (1962)

Rice, S. O.: Mathematical analysis of random noise. Bell Sys. Tech. J. **23**, 282-332 (1944)

Rossi, M. L., Prigioni, I., Valli, P., Casella, C.: Activation of the efferent system in the isolated frog labyrinth: effects on the afferent EPSPs and spike discharge recorded from single fibres of the posterior nerve. Brain Res. **185**, 125-137 (1980)

Rossi, M. L., Valli, P., Casella, C.: Post-synaptic potentials recorded from afferent nerve fibers of the posterior semicircular canal in the frog. Brain Res. **135**, 67-75 (1977)

Schessel, D. A.: Chemical Synaptic Transmission between Type I Vestibular Hair Cells and the Primary Afferent Nerve Chalice: An Intracellular Study Utilizing Horseradish Peroxidase. Ph.D. Dissertation. Bronx, N. Y.: Albert Einstein College of Medicine (1982)

Stein, R. B.: Some models of neuronal variability. Biophys. J. **7**, 37-68 (1967)

Tasaki, I.: New measurements of the capacity and resistance of the myelin sheath and the nodal membrane of the isolated frog nerve fiber. Am. J. Physiol. **181**, 639-650 (1955)

Walsh, B. T., Miller, J. B., Gacek, R. R., Kiang, N. Y. S.: Spontaneous activity in the eighth cranial nerve of the cat. Int. J. Neurosci. **3**, 221-236 (1972)

Yagi, T. Simpson, N. E., Markham, C. H.: The relationship of conduction velocity to other physiological properties of the cat's horizontal canal neurons. Exp. Brain Res. **30**, 587-600 (1977)

Legends to Figures

Fig. 1. Circuit for afterhyperpolarization model. See TEXT for symbols. The G_K conductance varies as a function of postspike time. The mean value of the G_S conductance remains constant for any steady-state condition, but varies as the condition of natural stimulation changes. An external current source, I_P, is included.

Fig. 2. A comparison between simulated and experimental interspike-interval statistics. The coefficient of variation (cv) is plotted against the mean interval ($\bar{t}$) for model units 1-5, as labelled on the graph. In this and other figures, units are identified as in Table 1. Points are from simulations with different values of g_S and with $V_P = 0$. The dashed curves are from simulations obtained by varying V_P with $\bar{g}_S$ set for each unit so that the mean interval in the absence of external galvanic currents is $\bar{t}_0 = 10$ ms. The solid curves are experimental relations, obtained from otolith neurons responding to natural stimulation (Goldberg et al., 1984). The simulated and experimental data are matched in terms of their cv*, the cv at a mean interval of 15 ms.

Fig. 3. Simulations of five consecutive interspike voltage trajectories for a regular neuron (model unit 2) in **A**, and for an irregular unit (model unit 5) in **B**. Spikes are arbitrarily drawn to have a duration of 0.5 ms. Horizontal dashed lines are the resting potential (0) and the critical firing level (V_T). The dotted curves on the third interspike interval for each unit are the mean voltage trajectories, $\mu_V(t)$. The values of $\bar{g}_S$ were .5347 and .1054 for units 2 and 5, respectively; the corresponding mean intervals, ignoring spike duration, were 10.1 and 9.9 ms.

Fig. 4. Simulated input-output curves for model units 1-5. **A**, discharge rate vs normalized synaptic input, $\bar{g}_S^* = \bar{g}_S \cdot [(V_S - V_T)/V_T]$. Vertical dashed line, $g_S^* = 1$. Points to the left of the dashed line represent nondeterministic firings, those to the right of the line, deterministic firings. **B**, response (measured as a change in discharge rate from rest) vs externally applied galvanic polarization (V_p). Positive values of V_p are excitatory; negative values, inhibitory. The mean interval when $V_p = 0$ was $\bar{t}_0 = 10$ ms in all cases V_p is in units of mV.

Fig. 5.A, simulated relations between sensitivity and discharge regularity (cv*). Solid and open symbols are sensitivity to externally applied galvanic currents (β_p) and to synaptic inputs (β_S), respectively. Units 1-5 (● or 0); units 3 A, B(▲ or Δ); and units 3C, D(■ or □). Straight lines are best-fitting power laws; regressions for units 3A, B and 3C, D included data for unit 3. **B**, lengthening effect (L_f on ordinate) vs fraction of mean interval (f on abscissa), based on unit 2. Simulated relations for $\bar{t}_0 = 7$ ms (upper dashed line), 10 ms (solid line) and 14 ms (lower dashed line). Each line is based on the t_f computed from 25 interposed spikes for each of seven, equally spaced values of f, ranging from 1/8 to 7/8. Solid points are experimental data with an average $\bar{t}_0$ near 10 ms (Goldberg et al., 1984).

Fig. 6. Recovery functions for the model. The short-shock threshold (V_p) is plotted against postspike time, measured as a fraction of the mean interval (f). Mean intervals are 7 (0), 10 (●) and 14 (x) ms for units 1 and 5 and 10 ms for unit 3. The solid curves were fit by eye to the 10 ms points. **A**, thresholds are calculated from

$V_P = [(V_T - \mu_V(t)] \cdot [1 + \bar{g}_S + g_K(t)]$. **B**, thresholds for a distributed model are shown as points and solid curves. The nerve fiber had an unmyelinated terminal, 50 μm long, continuous with a myelinated fiber, 8 mm long. Nodes were spaced every 200 μm. V_T was 10 mV for the terminal and 25 mV for the nodes. Length constants were 400 μm or two nodes for the myelinated fiber and 200 μm for the terminal when it was at rest ($g_S = 0$ and $g_K = 0$). Synaptic input was uniformly distributed along the terminal. A monopolar stimulating electrode was placed 1.0 mm from the fiber, opposite the first node or, equivalently, 200 μm from the proximal end of the terminal. The values of V_p were normalized so that $V_P = 1$ was the shock strength needed to depolarize the proximal end of the resting terminal by 1 mV. The dashed curve gives the thresholds if the spike always arose from the terminal. As expected, this corresponds closely to the recovery function for the original model. The solid curve and the points give the recovery functions for the distributed model; here, the spike starts at the first point along the nerve fiber to reach V_T as shock strength is raised. The two curves diverge when the spike originates from a node. They join when the spike begins in the terminal. The transition from one initiation site to the other occurs at f = 5/8 for unit 1 and f = 3/8 for unit 3. The spike always arises from the terminal for unit 5.

TABLE 1. Afterhyperpolarization model: parameters and response measures

	PARAMETERS				RESPONSE MEASURES					
Unit	N	g_{KO}	τ_K (ms)	A (mV)	cv*	$d\mu_V/dt$ (mV/ms)	σ_V (mV)	β_P (spikes·s^{-1}/mV)	β_S (spikes·s^{-1})	q
1	500	3.50	7.07	0.070	.0265	2.10	0.60	1.17	73.4	0. 70
2	500	2.15	6.50	0.136	.0476	1.69	0.92	2.11	131.7	0. 42
3	500	1.32	5.50	0.265	.0917	1.17	1.35	4.13	271.6	0.47
4	500	0.81	4.00	0.514	.2126	0.56	1.85	9.64	697.4	0.29
5	2500	0.50	2.36	1.000	.5082	0.11	2.25	26.46	2064.3	0.11
3A	500	1.32	5.50	0.070	.0574	1.17	0.69	4.28	268.2	0.47
3B	500	1.32	5.50	1.000	.1483	1.17	2.61	3.86	279.1	0.36
3C	500	3.50	7.07	0.265	.0452	2.10	1.16	1.15	73.9	0.44
3D	500	0.50	2.36	0.265	.4631	0.11	1.30	36.36	2451.5	0.10

N, number of intervals, each simulation run. Unit 5, based on two data sets of N = 500 and N = 2000. Values for unit 5 are weighted averages of the two sets. Other symbols are explained in TEXT. All response measures, except cv*, are for a mean interval, t_0 = 10 ms.

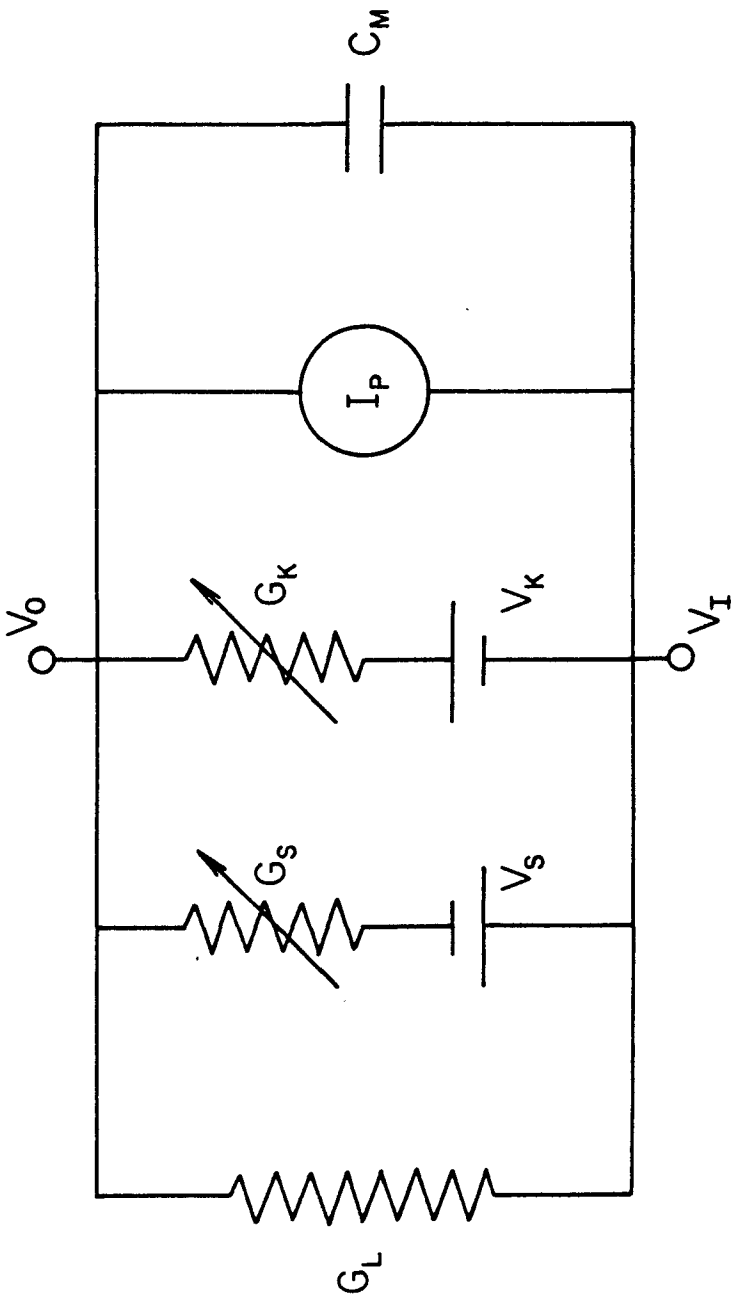

Figure 1

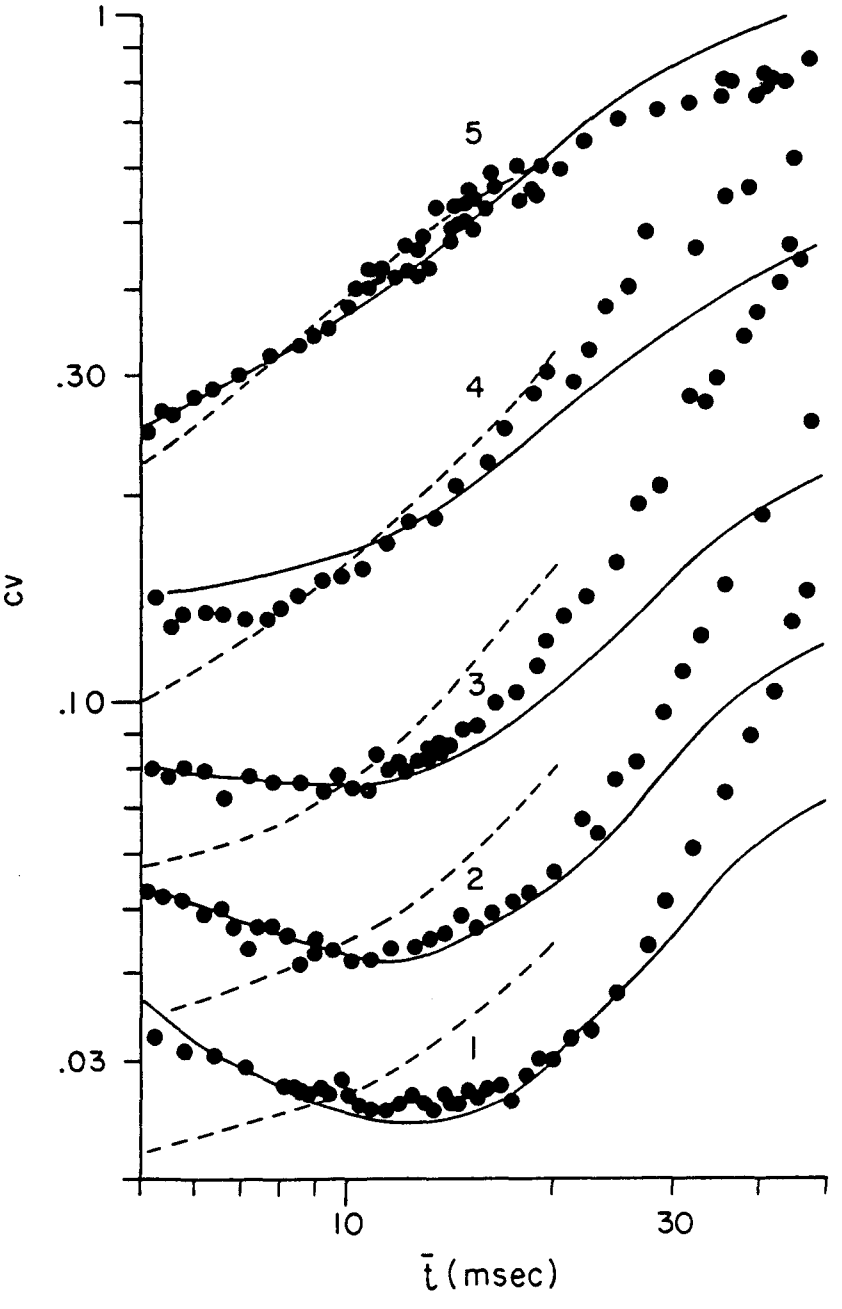

Figure 2

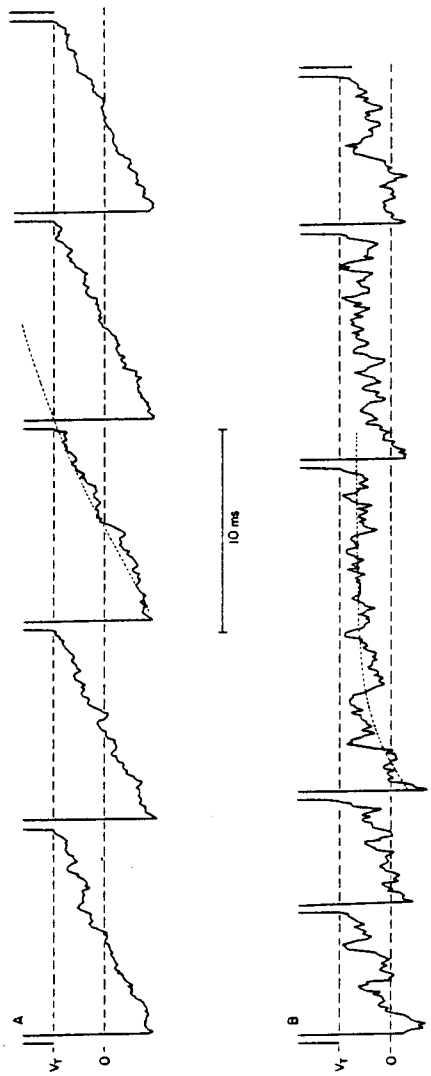

Figure 3

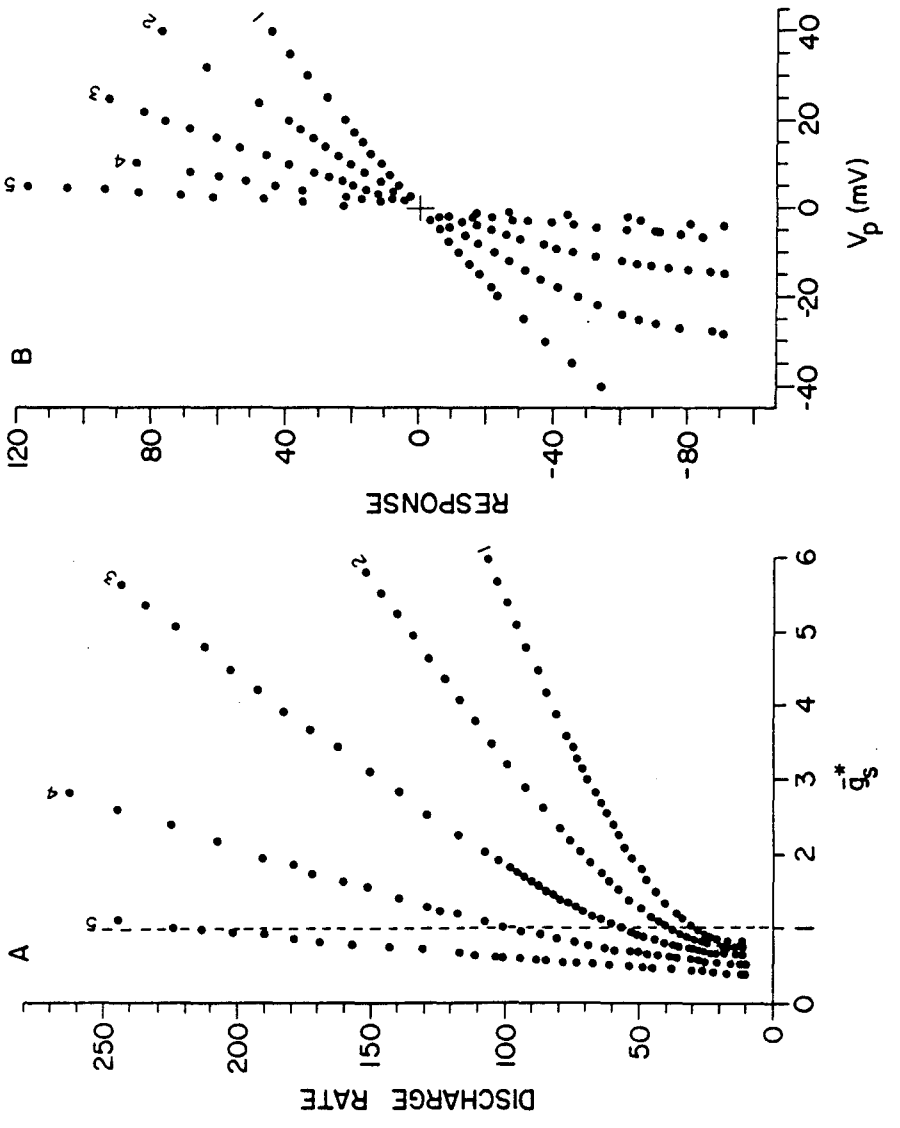

Figure 4

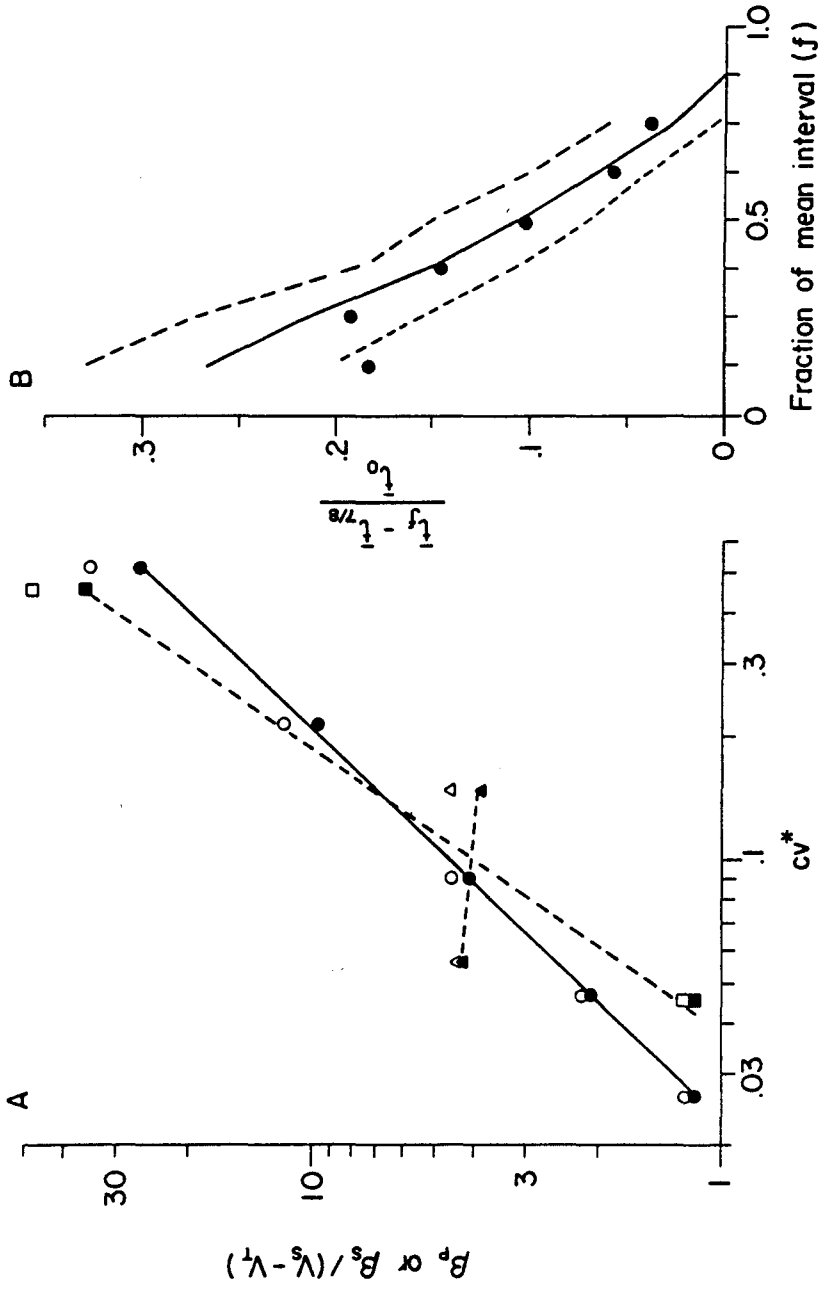
A
B
β_p or $\beta_s/(V_s-V_t)$
30
10
3
1
.03
.1
.3
cv*
$\frac{\bar{t}_f - \bar{t}_{T/2}}{\bar{t}_o}$
.3
.2
.1
0
0
0.5
1.0
Fraction of mean interval (f)

Figure 5

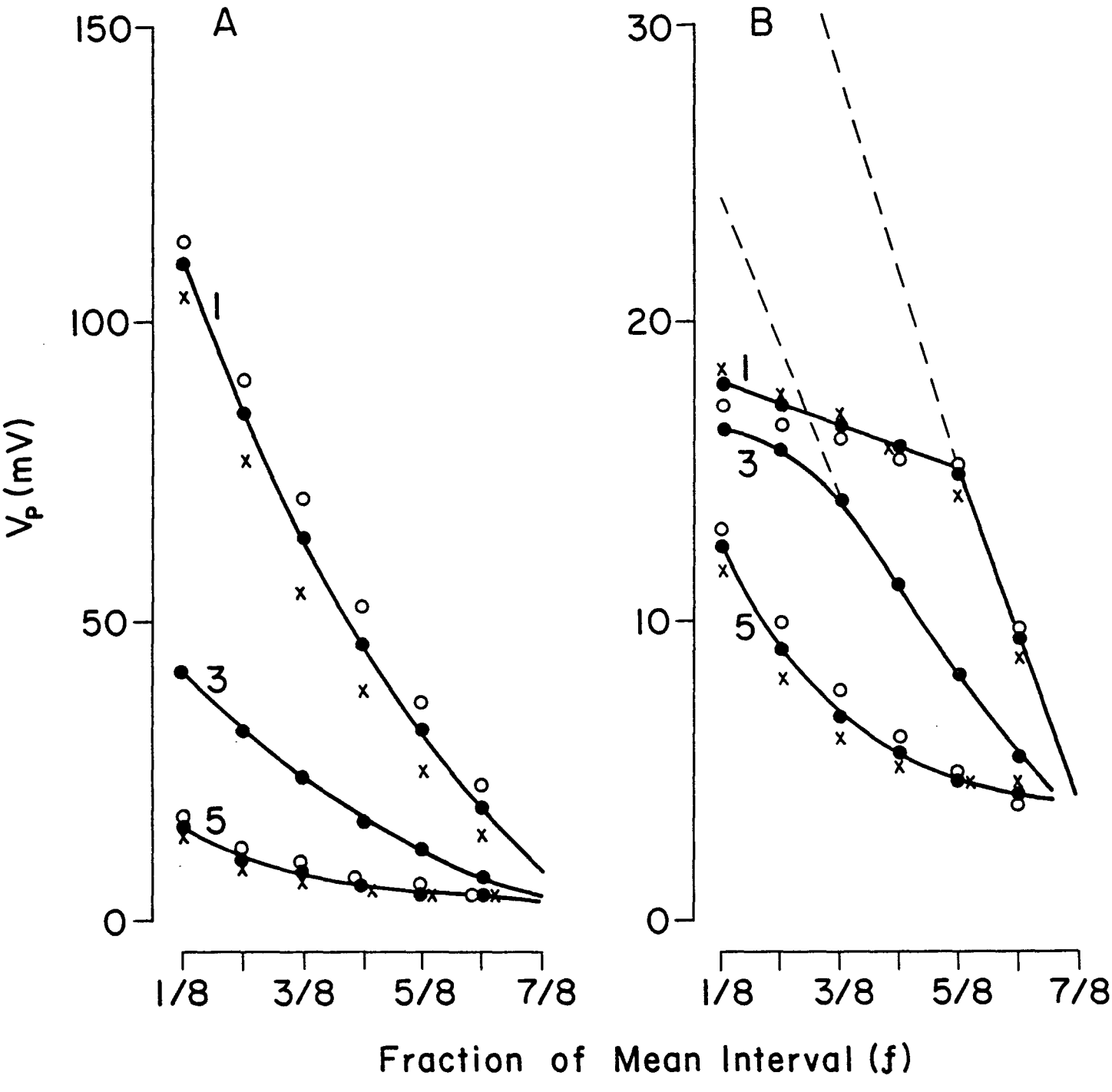
A
B
150
100
50
0
30
20
10
0
V_p (mV)
1
3
5
1/8
3/8
5/8
7/8
Fraction of Mean Interval (f)

Figure 6

SECURITY CLASSIFICATION OF THIS PAGE

REPORT DOCUMENTATION PAGE

1a. REPORT SECURITY CLASSIFICATION UNCLASSIFIED	1b. RESTRICTIVE MARKINGS
2a. SECURITY CLASSIFICATION AUTHORITY	3. DISTRIBUTION/AVAILABILITY OF REPORT Approved for Public Release: Distribution Unlimited
2b. CLASSIFICATION/DOWNGRADING SCHEDULE	
4. PERFORMING ORGANIZATION REPORT NUMBER(S) Mimeo Series No. 1671	5. MONITORING ORGANIZATION REPORT NUMBER(S)
6a. NAME OF PERFORMING ORGANIZATION N. C. State University 6b. OFFICE SYMBOL (*If applicable*) 4B855	7a. NAME OF MONITORING ORGANIZATION Office of Navy Research Department of the Navy
6c. ADDRESS (*City, State, and ZIP Code*) Dept. of Statistics Box 8203 Raleigh, N. C. 27695-8203	7b. ADDRESS (*City, State, and ZIP Code*) 800 North Quincy Street Arlington, Virginia 22217-5000
8a. NAME OF FUNDING/SPONSORING ORGANIZATION Office of Naval Research 8b. OFFICE SYMBOL (*If applicable*) ONR	9. PROCUREMENT INSTRUMENT IDENTIFICATION NUMBER N00014-85-K-0105
8c. ADDRESS (*City, State, and ZIP Code*) Department of the Navy 800 North Quincy Street Arlington, Virginia 22217-5000	10. SOURCE OF FUNDING NUMBERS PROGRAM ELEMENT NO. / PROJECT NO. / TASK NO. / WORK UNIT ACCESSION NO.

11. TITLE (*Include Security Classification*)
A Stochastic Afterhyperpolarization Model of Repetitive Activity in Vestibular Afferents (UNCLASSIFIED)

12. PERSONAL AUTHOR(S)
Charles E. Smith and Jay M. Goldberg

13a. TYPE OF REPORT	13b. TIME COVERED	14. DATE OF REPORT (*Year, Month, Day*)	15. PAGE COUNT
Technical	FROM ____ TO ____	October, 1985	35

16. SUPPLEMENTARY NOTATION

17. COSATI CODES			18. SUBJECT TERMS (*Continue on reverse if necessary and identify by block number*)
FIELD	GROUP	SUB-GROUP	

19. ABSTRACT (*Continue on reverse if necessary and identify by block number*)

A stochastic version of Kernell's (1968, 1972) model with cumulative after-hyperpolarization (AHP) was simulated. A characteristic of the model is that the AHP is the result of an increased potassium conductance (g_K) that is time-dependent but not voltage-dependent. Quantal synaptic inputs are assumed to be the only source of interspike-interval variability. The model reproduces many features of the steady-state discharge of peripheral vestibular afferents, provided that firing rates are higher than 40 spikes/s. Among the results accounted for are the interspike-interval statistics occurring during natural stimulation and their alteration by externally applied galvanic currents and the increase in the interspike interval following an interposed shock.

20. DISTRIBUTION/AVAILABILITY OF ABSTRACT	21. ABSTRACT SECURITY CLASSIFICATION
☒ UNCLASSIFIED/UNLIMITED ☐ SAME AS RPT. ☐ DTIC USERS	UNCLASSIFIED
22a. NAME OF RESPONSIBLE INDIVIDUAL	22b. TELEPHONE (*Include Area Code*) / 22c. OFFICE SYMBOL

DD FORM 1473, 84 MAR — 83 APR edition may be used until exhausted. All other editions are obsolete.

SECURITY CLASSIFICATION OF THIS PAGE
UNCLASSIFIED

Empirical studies show that some vestibular afferents have a regular spacing of action potentials, others an irregular spacing (Goldberg and Fernandez, 1971b; Fernandez and Goldberg, 1976). Irregularly discharging afferents have a higher sensitivity to externally applied galvanic currents than do regular afferents (Goldberg et al., 1984). To explain the relation between galvanic sensitivity and discharge regularity requires the assumption that neurons differ in both their synaptic noise (σ_V) and the slopes of their postspike voltage trajectories ($d\mu_V/dt$). The more irregular the neuron's discharge at a given firing frequency, the greater is σ_V and the smaller is $d\mu_V/dt$. Of the two factors, $d\mu_V/dt$ is estimated to be four times more influential in determining discharge regularity across the afferent population. The shortcomings of the model are considered, as are possible remedies. Our conclusions are compared to previous discussions of mechanisms responsible for differences in the discharge regularity of vestibular afferents.